First-principles determination of the structural, vibrational and thermodynamic properties of diamond, graphite, and derivatives

Nicolas Mounet* and Nicola Marzari†

Department of Materials Science and Engineering, Massachusetts Institute of Technology, Cambridge, Massachusetts 02139, USA
(Received 21 December 2004; published 31 May 2005)

The structural, dynamical, and thermodynamic properties of diamond, graphite and layered derivatives (graphene, rhombohedral graphite) are computed using a combination of density-functional theory total-energy calculations and density-functional perturbation theory lattice dynamics in the generalized gradient approximation. Overall, very good agreement is found for the structural properties and phonon dispersions, with the exception of the c/a ratio in graphite and the associated elastic constants and phonon dispersions. Both the C_{33} elastic constant and the Γ to A phonon dispersions are brought to close agreement with available data once the experimental c/a is chosen for the calculations. The vibrational free energy and the thermal expansion, the temperature dependence of the elastic moduli and the specific heat are calculated using the quasiharmonic approximation. Graphite shows a distinctive in-plane negative thermal-expansion coefficient that reaches its lowest value around room temperature, in very good agreement with experiments. Thermal contraction in graphene is found to be three times as large; in both cases, bending acoustic modes are shown to be responsible for the contraction, in a direct manifestation of the membrane effect predicted by Lifshitz over 50 years ago. Stacking directly affects the bending modes, explaining the large numerical difference between the thermal-contraction coefficients in graphite and graphene, notwithstanding their common physical origin.

I. INTRODUCTION

The extraordinary variety of carbon allotropes, as well as their present and potential applications in such diverse fields as nanoelectronics[1] or bioengineering,[2] gives them a special place among all elements. Even excluding fullerenes, nanotubes, and their derivatives, single crystalline diamond, graphite and graphene (i.e., a single graphite layer) still lack a complete characterization of their thermodynamic stability under a broad range of conditions (see, e.g., Refs. 3–7 and citations therein). In this respect, vibrational properties play a crucial role in determining the thermodynamic properties of the bulk. Indeed, diamond being a wide band gap material (E_g=5.5 eV), electronic excitations do not account for thermal properties up to high temperatures. Graphite and graphene are semimetals, but the gap vanishes only at the K point where the two massless bands cross (see, e.g., Ref. 8); thus, electronic excitations can often be neglected in these materials, and the phonon dispersions provide all the information that is needed to calculate thermodynamic quantities such as the thermal expansion or specific heat.

The aim of this paper is to provide a converged, accurate determination of the structural, dynamical, and thermodynamic properties of diamond, graphite, graphene, and rhombohedral graphite from first-principles calculations. Although the phonon spectrum of diamond and its thermal properties have been studied extensively with experiments[9,10] and calculations,[11] the phonon spectrum of graphite is still under active investigation,[12,13] as well as its thermal properties. Graphite in-plane thermal expansion has long been recognized to be negative,[14,15] and it has even been suggested[7,15] that this may be due to the internal stresses related to the large expansion in the c direction (Poisson effect). To resolve some of the open questions, and to provide a coherent theo-

retical picture for these materials, we used extensive *ab initio* density-functional theory (DFT) and density-functional perturbation theory (DFPT)[16,17] calculations. DFT is a very efficient and accurate tool to obtain ground-state and linear-response properties, especially when paired with plane-wave basis sets, which easily allow to reach full convergence with respect to basis size, and ultrasoft pseudopotentials[18] for optimal performance and transferability. We adopted the Perdew-Burke-Ernzerhof (PBE)[19] generalized gradient approximation (GGA) for the exchange-correlation functional, at variance with most of the early studies on diamond[11,20,21] and especially graphite,[13,22–26] which have been performed using the local density approximation (LDA). GGA calculations have appeared mostly for the cases of diamond (Ref. 21) and graphene (Refs. 12 and 13), with some data for graphite appearing in Refs. 13 and 27–29. DFPT (Refs. 16 and 17) is then used to compute the phonon frequencies at any arbitrary wave vector, without having to resort to the use of supercells. The vibrational free energy is calculated in the quasiharmonic approximation (QHA),[11,30] to predict finite-temperature lattice properties such as thermal expansion and specific heat.

To the best of our knowledge, this is the first study on the thermodynamic properties of graphite or graphene from first principles. For the case of diamond and graphene, calculations are fully *ab initio* and do not require any experimental input. For the case of graphite and rhombohedral graphite we argue that the use of the experimental c/a greatly improves the agreement with experimental data. This experimental input is required since DFT, in its current state of development, yields poor predictions for the interlayer interactions, dominated by van Der Waals dispersion forces not well described by local or semilocal exchange correlation functionals (see Refs. 31 and 32 for details; the agreement between LDA

predictions and experimental results for the c/a ratio is fortuitous). It is found that the weak interlayer bonding has a small influence on most of the properties studied and that forcing the experimental c/a corrects almost all the remaining ones. This allows us to obtain results for all the materials considered that are in very good agreement with the available experimental data.

The paper is structured as follows. We give a brief summary of our approach and definitions and introduce DFPT and the QHA in Sec. II. Our ground-state, zero-temperature results for diamond, graphite, graphene, and rhombohedral graphite are presented in Sec. III, lattice parameters and elastic constants from the equations of state in Sec. III A, phonon frequencies and vibrational density of states in Sec. III B, and first-principles, linear-response interatomic force constants in Sec. III C. The lattice thermal properties, such as thermal expansion, mode Grüneisen parameters, and specific heat as obtained from the vibrational free energy are presented in Sec. IV. Sec. V contains our final remarks.

II. THEORETICAL FRAMEWORK

A. Basics of density-functional perturbation theory

In density-functional theory[33,34] the ground state electronic density and wave functions of a crystal are found by solving self-consistently a set of one-electron equations. In atomic units (used throughout the paper), these are

$$\left[-\tfrac{1}{2}\nabla^2 + V_{\text{SCF}}(\mathbf{r})\right]|\psi_i\rangle = \varepsilon_i|\psi_i\rangle, \tag{1a}$$

$$V_{\text{SCF}}(\mathbf{r}) = \int \frac{n(\mathbf{r}')}{|\mathbf{r} - \mathbf{r}'|}d^3\mathbf{r}' + \frac{\delta E_{\text{xc}}}{\delta(n(\mathbf{r}))} + V_{\text{ion}}(\mathbf{r}), \tag{1b}$$

$$n(\mathbf{r}) = \sum_i |\psi_i(\mathbf{r})|^2 f(\varepsilon_F - \varepsilon_i), \tag{1c}$$

where $f(\varepsilon_F - \varepsilon_i)$ is the occupation function, ε_F the Fermi energy, E_{xc} the exchange-correlation functional (approximated by GGA-PBE in our case), $n(\mathbf{r})$ the electronic density, and $V_{\text{ion}}(\mathbf{r})$ the ionic core potential (actually a sum over an array of pseudopotentials).

Once the unperturbed ground state is determined, phonon frequencies can be obtained from the interatomic force constants, i.e., the second derivatives at equilibrium of the total crystal energy versus displacements of the ions,

$$C_{\alpha i,\beta j}(\mathbf{R} - \mathbf{R}') = \left.\frac{\partial^2 E}{\partial u_{\alpha i}(\mathbf{R})\partial u_{\beta j}(\mathbf{R}')}\right|_{\text{equil}} = C^{\text{ion}}_{\alpha i,\beta j}(\mathbf{R} - \mathbf{R}')$$
$$+ C^{\text{elec}}_{\alpha i,\beta j}(\mathbf{R} - \mathbf{R}'). \tag{2}$$

Here $\mathbf{R}$ ($\mathbf{R}'$) is a Bravais lattice vector, i (j) indicates the ith (jth) atom of the unit cell, and $\alpha(\beta)$ represents the Cartesian components. $C^{\text{ion}}_{\alpha i,\beta j}$ are the second derivatives[17] of Ewald sums corresponding to the ion-ion repulsion potential, while the electronic contributions $C^{\text{elec}}_{\alpha i,\beta j}$ are the second derivatives of the electron-electron and electron-ion terms in the ground state energy. From the Hellmann-Feynman theorem[17] one obtains

$$C^{\text{elec}}_{\alpha i,\beta j}(\mathbf{R} - \mathbf{R}') = \int \left[\frac{\partial n(\mathbf{r})}{\partial u_{\alpha i}(\mathbf{R})}\frac{\partial V_{\text{ion}}(\mathbf{r})}{\partial u_{\beta j}(\mathbf{R}')}\right.$$
$$\left. + n_0(\mathbf{r})\frac{\partial^2 V_{\text{ion}}(\mathbf{r})}{\partial u_{\alpha i}(\mathbf{R})\partial u_{\beta j}(\mathbf{R}')}\right]d^3\mathbf{r} \tag{3}$$

[where the dependence of both $n(\mathbf{r})$ and $V_{\text{ion}}(\mathbf{r})$ on the displacements has been omitted for clarity, and $V_{\text{ion}}(\mathbf{r})$ is considered local].

It is seen that the electronic contribution can be obtained from the knowledge of the linear response of the system to a displacement. The key assumption is then the Born-Oppenheimer approximation which views a lattice vibration as a static perturbation on the electrons. This is equivalent to say that the response time of the electrons is much shorter than that of ions, that is, each time ions are slightly displaced by a phonon, electrons instantaneously rearrange themselves in the state of minimum energy of the ionic configuration. Therefore, static linear response theory can be applied to describe the behavior of electrons upon a vibrational excitation.

For phonon calculations, we consider a periodic perturbation ΔV_{ion} of wave vector $\mathbf{q}$, which modifies the self-consistent potential V_{SCF} by an amount ΔV_{SCF}. The linear response in the charge density $\Delta n(\mathbf{r})$ can be found using first-order perturbation theory. If we consider its Fourier transform $\Delta n(\mathbf{q}+\mathbf{G})$, and calling $\psi_{o,\mathbf{k}}$ the one-particle wave function of an electron in the occupied band "o" at the point $\mathbf{k}$ of the Brillouin zone (and $\varepsilon_{o,\mathbf{k}}$ the corresponding eigenvalue), one can get a self-consistent set of linear equations similar to Eqs. (1a), (1b), and (1c),[35]

$$\left[\varepsilon_{o,\mathbf{k}} + \tfrac{1}{2}\nabla^2 - V_{\text{SCF}}(\mathbf{r})\right]\Delta\psi_{o,\mathbf{k}+\mathbf{q}} = \hat{P}_e^{\mathbf{k}+\mathbf{q}}\Delta V_{\text{SCF}}^{\mathbf{q}}\psi_{o,\mathbf{k}}, \tag{4a}$$

$$\Delta n(\mathbf{q}+\mathbf{G}) = \frac{4}{V}\sum_{\mathbf{k},o}\langle\psi_{e,\mathbf{k}}|e^{-i(\mathbf{q}+\mathbf{G})\cdot\mathbf{r}}\hat{P}_e^{\mathbf{k}+\mathbf{q}}|\Delta\psi_{o,\mathbf{k}+\mathbf{q}}\rangle, \tag{4b}$$

$$\Delta V_{\text{SCF}}(\mathbf{r}) = \int \frac{\Delta n(\mathbf{r}')}{|\mathbf{r} - \mathbf{r}'|}d^3\mathbf{r}' + \Delta n(\mathbf{r})\left[\frac{d}{dn}\left(\frac{\delta E_{\text{xc}}}{\delta(n(\mathbf{r}))}\right)\right]_{n_0(\mathbf{r})}$$
$$+ \Delta V_{\text{ion}}(\mathbf{r}). \tag{4c}$$

$\hat{P}_e^{\mathbf{k}+\mathbf{q}}$ refers to the projector on the empty-state manifold at $\mathbf{k}+\mathbf{q}$, V to the total crystal volume, and $\mathbf{G}$ to any reciprocal lattice vector. Note that the linear response contains only Fourier components of wave vector $\mathbf{q}+\mathbf{G}$, so we add a superscript $\mathbf{q}$ to $\Delta V_{\text{SCF}}^{\mathbf{q}}$. We implicitly assume for simplicity that the crystal has a band gap and that pseudopotentials are local, but the extension to the case of metals[36] or nonlocal pseudopotentials[17] is well established (see Ref. 16 for a detailed and complete review of DFPT).

Linear-response theory allows us to calculate the response to any periodic perturbation; i.e., it allows direct access to the dynamical matrix related to the interatomic force constants via a Fourier transform,

$$\tilde{D}_{\alpha i,\beta j}(\mathbf{q}) = \frac{1}{\sqrt{M_i M_j}} \sum_{\mathbf{R}} C_{\alpha i,\beta j}(\mathbf{R}) e^{-i\mathbf{q}\cdot\mathbf{R}} \qquad (5)$$

(where M_i is the mass of the ith atom).

Phonon frequencies at any $\mathbf{q}$ are the solutions of the eigenvalue problem

$$\omega^2(\mathbf{q}) u_{\alpha i}(\mathbf{q}) = \sum_{\beta j} u_{\beta j}(\mathbf{q}) \tilde{D}_{\alpha i,\beta j}(\mathbf{q}). \qquad (6)$$

In practice, one calculates the dynamical matrix on a relatively coarse grid in the Brillouin zone (say, a $8\times 8\times 8$ grid for diamond), and obtains the corresponding interatomic force constants by inverse Fourier transform (in this example it would correspond to a $8\times 8\times 8$ supercell in real space). Finally, the dynamical matrix (and phonon frequencies) at any $\mathbf{q}$ point can be obtained by Fourier interpolation of the real-space interatomic force constants.

B. Thermodynamic properties

When no external pressure is applied to a crystal, the equilibrium structure at any temperature T can be found by minimizing the Helmholtz free energy $F(\{a_i\},T)=U-TS$ with respect to all its geometrical degrees of freedom $\{a_i\}$. If now the crystal is supposed to be perfectly harmonic, F is the sum of the ground state total energy and the vibrational free energy coming from the partition function (in the canonical ensemble) of a collection of independent harmonic oscillators. In a straightforward manner, it can be shown[37] that

$$F(\{a_i\},T) = E(\{a_i\}) + F_{\mathrm{vib}}(T) = E(\{a_i\}) + \sum_{\mathbf{q},j} \frac{\hbar\omega_{\mathbf{q},j}}{2}$$
$$+ k_B T \sum_{\mathbf{q},j} \ln\left[1 - \exp\left(-\frac{\hbar\omega_{\mathbf{q},j}}{k_B T}\right)\right], \qquad (7)$$

where $E(\{a_i\})$ is the ground state energy and the sums run over all the Brillouin zone wave vectors and the band index j of the phonon dispersions. The second term on the right-hand side of Eq. (7) is the zero-point motion.

If anharmonic effects are neglected, the phonon frequencies do not depend on lattice parameters, and the free energy dependence on structure is entirely contained in $E(\{a_i\})$, energy of the static lattice as a function of the cell parameters. Thus, in a harmonic crystal, the structure does not depend on temperature. Thermal expansion is recovered by introducing in Eq. (7) the dependence of the phonon frequencies on the structural parameters $\{a_i\}$; direct minimization of the free energy

$$F(\{a_i\},T) = E(\{a_i\}) + F_{\mathrm{vib}}(\omega_{\mathbf{q},j}(\{a_i\}),T)$$
$$= E(\{a_i\}) + \sum_{\mathbf{q},j} \frac{\hbar\omega_{\mathbf{q},j}(\{a_i\})}{2}$$
$$+ k_B T \sum_{\mathbf{q},j} \ln\left[1 - \exp\left(-\frac{\hbar\omega_{\mathbf{q},j}(\{a_i\})}{k_B T}\right)\right] \qquad (8)$$

provides the equilibrium structure at any temperature T. This approach goes under the name quasiharmonic approximation

and has been applied successfully to many bulk systems.[11,38,39] The linear thermal expansion coefficients of the cell dimensions of a lattice are then

$$\alpha_i = \frac{1}{a_i}\frac{\partial a_i}{\partial T}. \qquad (9)$$

The Grüneisen formalism[40] assumes a linear dependence of the phonon frequencies on three orthogonal cell dimensions $\{a_i\}$; developing the ground state energy up to second order one can get from the condition $(\partial F/\partial a_i)_T=0$ the alternative expression

$$\alpha_i = \sum_{\mathbf{q},j} c_v(\mathbf{q},j) \sum_k \frac{S_{ik}}{V_0}\left(\frac{-a_{0,k}}{\omega_{0,\mathbf{q},j}}\left.\frac{\partial\omega_{\mathbf{q},j}}{\partial a_k}\right|_0\right). \qquad (10)$$

We follow here the formalism of Ref. 41: $c_v(\mathbf{q},j)$ is the contribution to the specific heat from the mode $(\mathbf{q},j)$, S_{ik} is the elastic compliance matrix, and the subscript "0" indicates a quantity taken at the ground state lattice parameter. The Grüneisen parameter of the mode $(\mathbf{q},j)$ is by definition

$$\gamma_k(\mathbf{q},j) = \frac{-a_{0,k}}{\omega_{0,\mathbf{q},j}}\left.\frac{\partial\omega_{\mathbf{q},j}}{\partial a_k}\right|_0. \qquad (11)$$

For a structure which depends only on one lattice parameter a (e.g., diamond or graphene) one then gets for the linear thermal expansion coefficient

$$\alpha = \frac{1}{a_0^2 \left.\dfrac{\partial^2 E}{\partial a^2}\right|_0}\sum_{\mathbf{q},j} c_v(\mathbf{q},j)\frac{-a_0}{\omega_{0,\mathbf{q},j}}\left.\frac{\partial\omega_{\mathbf{q},j}}{\partial a}\right|_0. \qquad (12)$$

Note that $a_0^2\,(\partial^2 E/\partial a^2)|_0 = 9V_0 B_0$ for diamond, where B_0 is the bulk modulus and V_0 the equilibrium volume of the primitive cell.

In the case of graphite there are two lattice parameters, a in the basal plane and c perpendicular to the basal plane, so that one gets

$$\alpha_a = \frac{1}{V_0}\sum_{\mathbf{q},j} c_v(\mathbf{q},j)\left((S_{11}+S_{12})\frac{-a_0}{2\omega_{0,\mathbf{q},j}}\left.\frac{\partial\omega_{\mathbf{q},j}}{\partial a}\right|_0\right.$$
$$\left. + S_{13}\frac{-c_0}{\omega_{0,\mathbf{q},j}}\left.\frac{\partial\omega_{\mathbf{q},j}}{\partial c}\right|_0\right), \qquad (13a)$$

$$\alpha_c = \frac{1}{V_0}\sum_{\mathbf{q},j} c_v(\mathbf{q},j)\left(S_{13}\frac{-a_0}{\omega_{0,\mathbf{q},j}}\left.\frac{\partial\omega_{\mathbf{q},j}}{\partial a}\right|_0 + S_{33}\frac{-c_0}{\omega_{0,\mathbf{q},j}}\left.\frac{\partial\omega_{\mathbf{q},j}}{\partial c}\right|_0\right). \qquad (13b)$$

The mode Grüneisen parameters provide useful insight in the thermal expansion mechanisms. They are usually positive, since phonon frequencies decrease when the solid expands, although some negative mode Grüneisen parameters for low-frequency acoustic modes can arise and sometimes compete with positive ones, giving a negative thermal expansion at low temperatures, when only the lowest acoustic modes can be excited.

Finally, the heat capacity per unit cell at constant volume can be obtained from $C_v = -T(\partial^2 F_{\mathrm{vib}}/\partial T^2)_V$,[37]

	Present calculation	Experiment (300 K)
Lattice constant a_0	6.743 (GS)	6.740[a]
(a.u.)	6.769 (300 K)	
Bulk modulus B_0	432 (GS)	442 ± 2[b]
(GPa)	422 (300 K)	

[a]Reference 49.
[b]Reference 50.

$$C_v = \sum_{\mathbf{q},j} c_v(\mathbf{q},j) = k_B \sum_{\mathbf{q},j} \left(\frac{\hbar\omega_{\mathbf{q},j}}{2k_B T}\right)^2 \frac{1}{\sinh^2\left(\frac{\hbar\omega_{\mathbf{q},j}}{2k_B T}\right)}. \quad (14)$$

C. Computational details

All the calculations that follow are performed using the ν-ESPRESSO (Ref. 42) package, which is a full *ab initio* DFT and DFPT code available under the GNU General Public License.[43] We use a plane-wave basis set, ultrasoft pseudopotentials[18] from the standard distribution[44] [generated using a modified RRKJ (Ref. 45) approach], and the generalized gradient approximation in its PBE parametrization[19] for the exchange-correlation functional. We also use the local density approximation (LDA) in order to compare some results between the two functionals. In this case the parametrization used is the one proposed by Perdew and Zunger.[46]

For the semimetallic graphite and graphene cases, we use 0.03 Ry of cold smearing.[47] We carefully and extensively check the convergence in the energy differences between different configurations and the phonon frequencies with respect to the wave function cutoff, the dual (i.e., the ratio between charge density cutoff and wave function cutoff), the k-point sampling of the Brillouin zone, and the interlayer vacuum spacing for graphene. Energy differences are converged within 5 meV/atom or better, and phonon frequencies within $1-2$ cm^{-1}. In the case of graphite and graphene phonon frequencies are converged with respect to the k-point sampling after having set the smearing parameter at 0.03 Ry. Besides, values of the smearing between 0.02 Ry and 0.04 Ry do not change the frequencies by more than $1-2$ cm^{-1}.

In a solid, translational invariance guaranties that three phonon frequencies at Γ will go to zero. In our GGA-PBE DFPT formalism this condition is exactly satisfied only in the limit of infinite k-point sampling and full convergence with the plane-wave cutoffs. For the case of graphene and graphite we find in particular that an exceedingly large cutoff (100 Ry) and dual (28) would be needed to recover phonon dispersions (especially around Γ and the Γ-A branch) with the tolerances mentioned; on the other hand, application of the acoustic sum rule (i.e., forcing the translational symmetry on the interatomic force constants) allows us to recover these
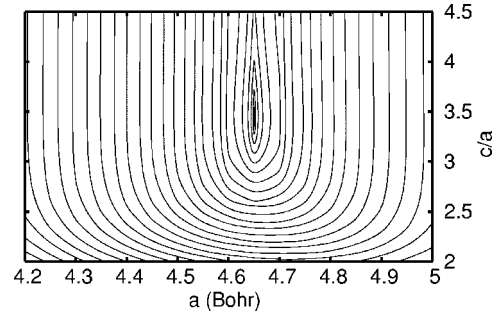

FIG. 1. Contour plot of the ground state energy of graphite as a function of a and c/a (isoenergy contours are not equidistant).

highly converged calculations with a more reasonable cutoff and dual.

Finally, the cutoffs used are 40 Ry for the wave functions in all the carbon materials presented, with duals of 8 for diamond and 12 for graphite and graphene, corresponding to a charge density cutoff of 320 Ry for diamond and 480 Ry for graphite and graphene. We use a $8 \times 8 \times 8$ Monkhorst-Pack mesh for the Brillouin zone sampling in diamond, 16 $\times 16 \times 8$ in graphite, $16 \times 16 \times 4$ in rhombohedral graphite and $16 \times 16 \times 1$ in graphene. All these meshes are not shifted (i.e., they include Γ). The dynamical matrix is explicitly calculated on a $8 \times 8 \times 8$ q-points mesh in diamond, $8 \times 8 \times 4$ in graphite, $8 \times 8 \times 2$ in rhombohedral graphite and $16 \times 16 \times 1$ in graphene. Finally, integrations over the Brillouin zone for the vibrational free energy or the heat capacity are done using phonon frequencies that are Fourier interpolated on much finer meshes. The phonon frequencies are usually computed at several lattice parameters and the results interpolated to get their dependence on lattice constants.

A final remark is that we are careful to use the same parameters (cutoffs, k-points sampling, smearing, etc.) in the determination of the ground state (static) energy and that of the phonon frequencies, since these two terms need to be added in the free energy expression.

III. ZERO-TEMPERATURE RESULTS

A. Structural and elastic properties

We perform ground state total-energy calculations on diamond, graphite, and graphene over a broad range of lattice parameters. The potential energy surface is then fitted by an appropriate equation of state, and its minimum provides theoretical predictions for the ground state equilibrium lattice parameter(s). The second derivatives at the minimum are related to the bulk modulus and elastic constants.

For the case of diamond we choose the Birch equation of state[48] (up to the fourth order) to fit the total energy vs the lattice constant a,

$$E(a) = -E_0 + \frac{9}{8} B_0 V_0 \left[\left(\frac{a_0}{a}\right)^2 - 1\right]^2 + A\left[\left(\frac{a_0}{a}\right)^2 - 1\right]^3$$
$$+ B\left[\left(\frac{a_0}{a}\right)^2 - 1\right]^4 + \mathcal{O}\left[\left(\frac{a_0}{a}\right)^2 - 1\right]^5, \quad (15)$$
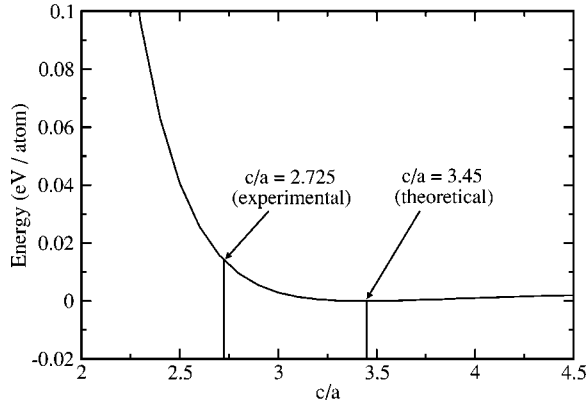
FIG. 2. Ground state energy of graphite as a function of c/a at fixed $a=4.65$ a.u.. The theoretical (PBE) and the experimental c/a are shown. The zero of energy is set to the PBE minimum.

$$\text{stiffness coefficients}\begin{cases} C_{11}+C_{12}=\dfrac{1}{\sqrt{3}c_0}\dfrac{\partial^2 E}{\partial a^2}, \\[8pt] C_{33}=\dfrac{2c_0}{\sqrt{3}a_0^2}\dfrac{\partial^2 E}{\partial c^2}, \\[8pt] C_{13}=\dfrac{1}{\sqrt{3}a_0}\dfrac{\partial^2 E}{\partial a\,\partial c}, \end{cases}$$

(16a)

$$\text{tetragonal shear modulus }C^t=\tfrac{1}{6}[(C_{11}+C_{12})+2C_{33}-4C_{13}],$$

(16b)

$$\text{bulk modulus }B_0=\frac{C_{33}(C_{11}+C_{12})-2C_{13}^2}{6C^t}.$$ (16c)

where B_0 is the bulk modulus, V_0 the primitive cell volume ($V_0=a_0^3/4$ here) and A and B are fit parameters. The Murnaghan equation of state or even a polynomial would fit equally well the calculations around the minimum of the curve. A best fit of this equation on our data gives us both the equilibrium lattice parameter and the bulk modulus; our results are summarized in Table I. The agreement with the experimental values is very good, even after the zero-point motion and thermal expansion are added to our theoretical predictions (see Sec. IV).

The equation of state for graphene is fitted by a fourth order polynomial, and the minimum found for $a=4.654$ a.u., which is very close to the experimental in-plane lattice parameter of graphite. The graphite equation of state is fitted by a two-dimensional fourth order polynomial in the variables a and c. To illustrate the very small dependence of the ground state energy with the c/a ratio, we plot the results of our calculations over a broad range of lattice constants in Figs. 1 and 2. A few elastic constants can be obtained from the second derivatives of this energy,[22]

We summarize all our LDA and GGA results in Table II. For LDA, both the lattice parameter a_0 and the c_0/a_0 ratio are very close to experimental data. Elastic constants are calculated fully from first principles, in the sense that the second derivatives of the energy are taken at the theoretical LDA a_0 and c_0, and that only these theoretical values are used in Eqs. (16a). Elastic constants are found in good agreement with experiments, except for the case of C_{13} which comes out as negative (meaning that the Poisson's coefficient would be negative). Fully theoretical GGA results (second column of Table II) compare poorly to experimental data except for the a_0 lattice constant, in very good agreement with experiments. Using the experimental value for c_0 in Eqs. (16a) improves only the value of $C_{11}+C_{12}$ (third column of Table II). Most of the remaining disagreement is related to the poor value obtained for c/a; if the second derivatives in Eqs. (16a) are taken at the experimental value for c/a all elastic constants are accurately recovered except for C_{13} (fourth column of Table II). In both LDA and GGA, errors arise from the fact that van Der Waals interactions between graphitic layers are poorly described. These issues can still be addressed within the framework of DFT (as shown by

TABLE II. Structural and elastic properties of graphite according to LDA, GGA, and experiments.

	LDA fully theoretical	GGA fully theoretical	GGA using Expt. c_0 in Eqs. (16a)	GGA with second derivatives taken at Expt. c_0/a_0	Experiment (300 K)
Lattice constant a_0(a.u.)	4.61	4.65	4.65	4.65 (fixed)	4.65±0.003[a]
c_0/a_0 ratio	2.74	3.45	3.45	2.725(fixed)	2.725±0.001[a]
$C_{11}+C_{12}$ (GPa)	1283	976	1235	1230	1240±40[b]
C_{33} (GPa)	29	2.4	1.9	45	36.5±1[b]
C_{13} (GPa)	−2.8	−0.46	−0.46	−4.6	15±5[b]
B_0 (GPa)	27.8	2.4	1.9	41.2	35.8[c]
C^t (GPa)	225	164	207	223	208.8[c]

[a]References 51–53, as reported by Ref. 22.
[b]Reference 6.
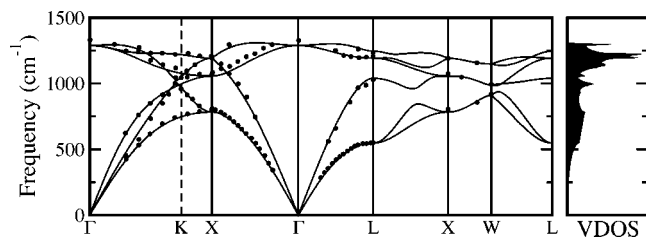[c]Reference 54, as reported by Ref. 22.

FIG. 3. GGA *ab initio* phonon dispersions (solid lines) and vibrational density of states (VDOS) for diamond. Experimental neutron scattering data from Ref. 9 are shown for comparison (circles).

Langreth and collaborators, Ref. 31) at the cost of having a nonlocal exchange-correlation potential.

Zero-point motion and finite-temperature effects will be discussed in details in Sec. IV.

B. Phonon dispersion curves

We calculate the phonon dispersion relations for diamond, graphite, rhombohedral graphite and graphene. For diamond and graphene, we use the theoretical lattice parameter. For graphite, we either use the theoretical c/a or the experimental one ($c/a = 2.725$). We will comment in the following on the role of c/a on our calculated properties. Finally we also calculate the phonon dispersions for rhombohedral graphite, which differs from graphite only in the stacking of the parallel layers, in graphite the stacking is *ABABAB* while it is *ABCABC* in rhombohedral graphite, and the latter unit cell contains six atoms instead of four. We therefore use the same in-plane lattice parameter and same interlayer distance as in graphite (that is, a c/a ratio multiplied by 1.5). Results are presented in Figs. 3, 4, 5, 6, and 7, and in Table III and IV, together with the experimental data.

In diamond, GGA produces softer modes than LDA (Ref. 11) on the whole (as expected), particularly at Γ (optical mode) and in the optical Γ-X branches. For these, the agree-
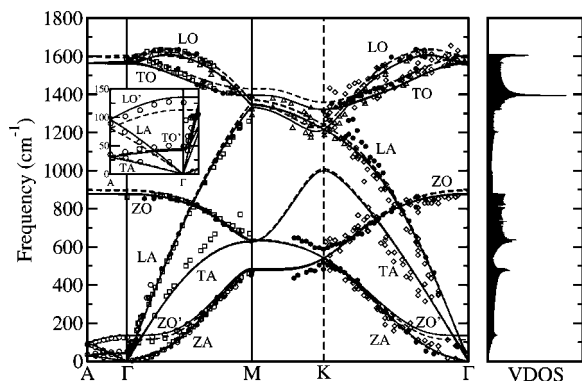

FIG. 4. GGA (solid lines) and LDA (dashed line) *ab initio* phonon dispersions for graphite, together with the GGA vibrational density of states (VDOS). The inset shows an enlargement of the low-frequency Γ-A region. The experimental data are EELS (electron energy loss spectroscopy) from Refs. 55, 56, and 57 (respectively squares, diamonds, and filled circles), neutron scattering from Ref. 58 (open circles), and x-ray scattering from Ref. 12 (triangles). Data for Refs. 55 and 57 are taken from Ref. 13.
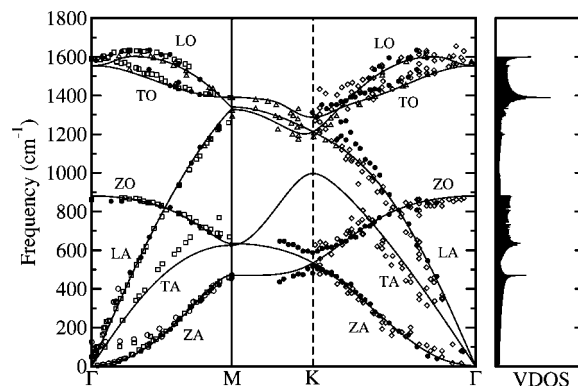

FIG. 5. GGA *ab initio* phonon dispersions for graphene (solid lines). Experimental data for graphite are also shown, as in Fig. 4.

ment is somehow better in LDA; on the other hand, the whole Γ-L dispersion is overestimated by LDA.

The results on graphite require some comments. In Table IV and Figs. 4–7, modes are classified as follows: L stands for longitudinal polarization, T for in-plane transversal polarization and Z for out-of-plane transversal polarization. For graphite, a prime (as in LO$'$) indicates an optical mode where the two atoms in each layer of the unit cell oscillate together and in phase opposition to the two atoms of the other layer. A nonprimed optical mode is instead a mode where atoms inside the same layer are "optical" with respect to each other. Of course "primed" optical modes do not exist for graphene, since there is only one layer (two atoms) per unit cell.

We observe that stacking has a negligible effect on all the frequencies above 400 cm^{-1}, since both rhombohedral graphite and hexagonal graphite show nearly the same dispersions except for the Γ-A branch and the in-plane dispersions near Γ. The in-plane part of the dispersions is also very similar to that of graphene, except of course for the low optical branches (below 400 cm^{-1}) that appear in graphite and are not present in graphene.

For graphite as well as diamond GGA tends to underestimate high optical modes while LDA overestimates them. The opposite happens for the low optical modes, and for the Γ-A branch of graphite; the acoustic modes show marginal
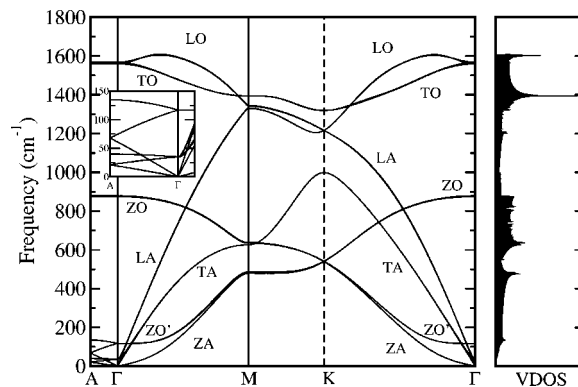

FIG. 6. GGA *ab initio* phonon dispersions for rhombohedral graphite. The inset shows an enlargement of the low-frequency Γ-A region.
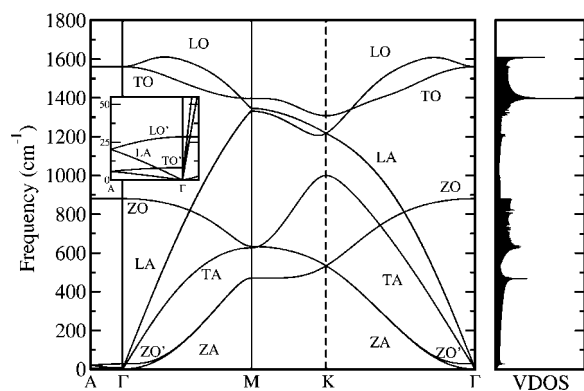
FIG. 7. GGA *ab initio* phonon dispersions for graphite at the theoretical c/a. The inset shows an enlargement of the low-frequency Γ-A region.

differences and are in very good agreement with experiments. Overall, the agreement of both LDA and GGA calculations with experiments is very good and comparable to that between different measurements.

Some characteristic features of both diamond and graphite are well reproduced by our *ab initio* results, such as the LO branch overbending and the associated shift of the highest frequencies away from Γ. Also, in the case of graphite, rhombohedral graphite and graphene, the quadratic dispersion of the in-plane ZA branch in the vicinity of Γ is observed; this is a characteristic feature of the phonon dispersions of layered crystals,[60,61] observed experimentally, e.g., with neutron scattering.[58] Nevertheless, some discrepancies are found in graphite. The most obvious one is along the Γ-M TA branch, where EELS (Ref. 55) data show much higher frequencies than calculations. Additionally several EELS experiments[56,57] report a gap between the ZA and ZO branches at K while these cross each other in all the calculations. In these cases the disagreement could come either from a failure of DFT within the approximations used or from imperfections in the crystals used in the experiments. There are also discrepancies between experimental data, in particular in graphite for the LA branch around K: EELS data from Ref. 56 agree with our *ab initio* results while those from Ref. 57 deviate from them.

We should stress again the dependence of the graphite phonon frequencies on the in-plane lattice parameter and c/a ratio. The results we have analyzed so far and that we are going to use in the remaining sections are obtained using the theoretical in-plane lattice parameter a and the experimental c/a ratio for both GGA and LDA. For GGA, calculations

performed at the theoretical c/a (3.45 instead of 2.725) strongly underestimate low-frequency modes (below 150 cm^{-1}) especially between Γ and A, as can be seen in Fig. 7 and in the second column of Table IV. High-frequency optical modes are not significantly affected by this change in c/a, but still depend on the in-plane lattice constant a; this explains much of the discrepancy between the LDA optical modes and the GGA ones (calculated at the equilibrium a =4.61 and a=4.65, respectively).

Finally, elastic constants can be extracted from the data on sound velocities. Indeed, the latter are the slopes of the dispersion curves in the vicinity of Γ and can be expressed as the square root of linear combinations of elastic constants (depending on the branch considered) over the density (see Ref. 62 for details). We note in passing that we compute the density consistently with the geometry used in the calculations (see Table IV for details, first column for LDA and third one for GGA), and not the experimental density. Our results are shown in Table V. The overall agreement with experiment is good to very good. LDA leads to larger elastic constants, as expected from the general tendency to "overbind," but still agrees well with experiment. For diamond, the agreement is particularly good. As for C_{13} in graphite, it is quite difficult to obtain it from the dispersion curves since it enters the sound velocities only in a linear combination involving other elastic constants, for which the error is almost comparable to the magnitude of C_{13} itself.

An accurate description of the phonon dispersions allows us to predict the low-energy structural excitations and thus several thermodynamic quantities. Before exploring this in Sec. IV, we want to discuss the nature and decay of the interatomic force constants in carbon-based materials.

C. Interatomic force constants

As explained in Sec. II A, the interatomic force constants $C_{i,j}(\mathbf{R}-\mathbf{R}')$ are obtained in our calculations from the Fourier transform of the dynamical matrix $\tilde{D}_{i,j}(\mathbf{q})$ calculated on a regular mesh inside the Brillouin zone ($8 \times 8 \times 8$ for diamond and $16 \times 16 \times 1$ for graphene). At a given $\mathbf{R}$, $C_{i,j}(\mathbf{R})$ is actually a second order tensor, and the decay of its norm (defined as the square root of the sum of the squares of all the matrix elements) with distance is a good measure of the long-range effects coming from distant neighbors. In Fig. 8 we plot the natural logarithm of such a norm with respect to the distance from a given atom, for the cases of diamond and graphene. In diamond the decay of the force constants along (110) is much slower than in other directions due to long-

TABLE III. Phonon frequencies of diamond at the high-symmetry points Γ, X, and L, in cm^{-1}.

	Γ_O	X_{TA}	X_{TO}	X_{LO}	L_{TA}	L_{LA}	L_{TO}	L_{LO}
LDA[a]	1324	800	1094	1228	561	1080	1231	1275
GGA[b]	1289	783	1057	1192	548	1040	1193	1246
Expt.[c]	1332	807	1072	1184	550	1029	1206	1234

[a]Reference 11.
[b]Present calculation.
[c]Reference 9.

TABLE IV. Phonon frequencies of graphite and derivatives at the high-symmetry points A, Γ, M, and K, in cm^{-1}. The lattice constants used in the calculations are also shown.

	Graphite			Rhombo. graphite	Graphene	Graphite
Functional	LDA	GGA	GGA	GGA	GGA	Experiment
In-plane lattice constant a_0	4.61 a.u.	4.65 a.u.	4.65 a.u.	4.65 a.u.	4.65 a.u.	4.65 a.u.
Interlayer distance/a_0	1.36	1.725	1.36	1.36	15	1.36
$A_{TA/TO'}$	31	6	29			35[a]
$A_{LA/LO'}$	80	20	96			89[a]
A_{LO}	897	880	878			
A_{TO}	1598	1561	1564			
$\Gamma_{LO'}$	44	8	41	35		49[a]
$\Gamma_{ZO'}$	113	28	135	117		95[b], 126[a]
Γ_{ZO}	899	881	879	879	881	861[b]
$\Gamma_{LO/TO}$	1593	1561	1559	1559	1554	1590[b], 1575[f]
	1604	1561	1567			
M_{ZA}	478	471	477	479	471	471[a], 465[b], 451[d]
M_{TA}	630	626	626	626	626	630[d]
M_{ZO}	637	634	634	635	635	670[b]
M_{LA}	1349	1331	1330	1330	1328	1290[c]
M_{LO}	1368	1346	1342	1344	1340	1321[c]
M_{TO}	1430	1397	1394	1394	1390	1388[c], 1389[b]
K_{ZA}	540	534	540	535	535	482[d], 517[d], 530[e]
K_{ZO}	544	534	542	539	535	588[d], 627[e]
K_{TA}	1009	999	998	998	997	
$K_{LA/LO}$	1239	1218	1216	1216	1213	1184[c], 1202[c]
K_{TO}	1359	1308	1319[g]	1319	1288[g]	1313[d], 1291[e]

[a]Reference 58.
[b]Reference 55.
[c]Reference 12.
[d]Reference 57.
[e]Reference 56.
[f]Reference 59.
[g]Note that a direct calculation of this mode with DFPT (instead of the Fourier interpolation result given here) leads to a significantly lower value in the case of graphite—1297 cm^{-1} instead of 1319 cm^{-1}. This explains much of the discrepancy between the graphite and graphene result, since in the latter we use a denser q-points mesh. This effect is due to the Kohn anomaly occurring at K (Ref. 29).

TABLE V. Elastic constants of diamond and graphite as calculated from the phonon dispersions, in GPa.

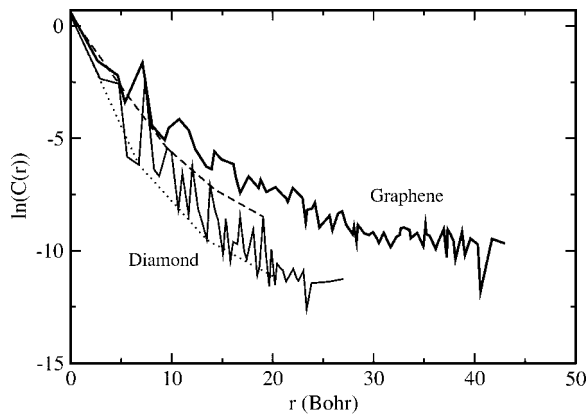|	Diamond		Graphite		
Functional	GGA	Expt.	LDA	GGA	Expt.
C_{11}	1060	1076.4±0.2[a]	1118	1079	1060±20[b]
C_{12}	125	125.2±2.3[a]	235	217	180±20[b]
C_{44}	562	577.4±1.4[a]	4.5	3.9	4.5±0.5[b]
C_{33}			29.5	42.2	36.5±1[b]

[a]Reference 50.
[b]Reference 6.

FIG. 8. Decay of the norm of the interatomic force constants as a function of distance for diamond (thin solid line) and graphene (thick solid line), averaged over all directions and in a semilogarithmic scale. The dotted line shows the decay for diamond along the (100) direction, and the dashed line that along the (110) direction.

range elastic effects along the covalent bonds. This long-range interaction is also responsible for the flattening of the phonon dispersions in zinc-blende and diamond semiconductors along the K-X line (see, e.g., Fig. 3 and Ref. 17). The force-constants decay in graphene is slower than in diamond and it depends less on direction. Note that in graphite the force constants (not represented here) include values corresponding to graphene (in-plane nearest neighbors) and smaller values corresponding to weak interlayer interactions.

It is interesting to assess the effects of truncation of these interatomic force constants on the phonon dispersions. Figures 9 and 10 show the change in frequency for selected modes in diamond and graphene as a function of the truncation range. The modes we chose are those most strongly affected by the number of neighbors included.

For diamond, our whole supercell contains up to 47 neighbors, and the graph shows only the region up to 20 neighbors included, since the selected modes do not vary by more than 1 cm^{-1} after that. With five neighbors, phonon frequencies are already near their converged value, being off by at worst 4%; very good accuracy (5 cm^{-1}) is obtained with 13 neighbors.
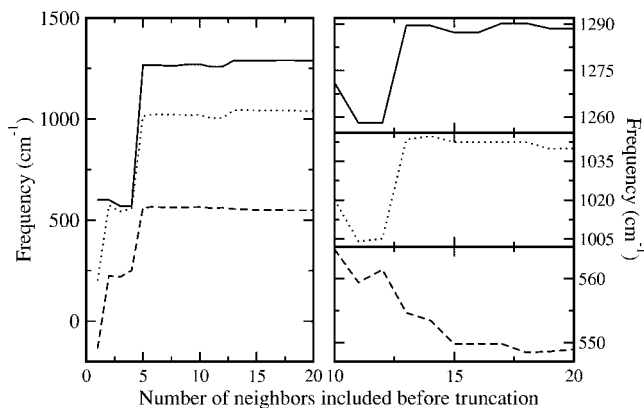
FIG. 9. Phonon frequencies of diamond as a function of the number of neighbors included in the interatomic force constants, Γ_O (solid line), X_{TO} (dotted line), and L_{TA} (dashed line).
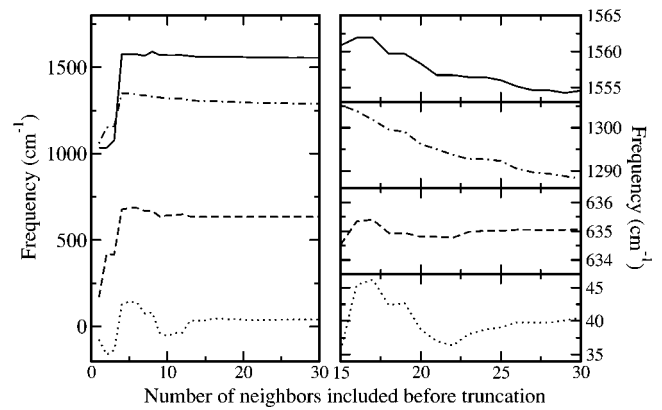
FIG. 10. Phonon frequencies of graphene as a function of the number of neighbors included in the interatomic force constants, $\Gamma_{LO/TO}$ (solid line), K_{TO} (dotted-dashed), M_{ZO} (dashed), and for the dotted line a phonon mode in the ZA branch one-fourth along the Γ to M line.

For graphene, our $16 \times 16 \times 1$ supercell contains up to 74 neighbors, but after the 30th no relevant changes occur. At least 4 neighbors are needed for the optical modes to be converged within 5%–8%. On the other hand, the frequency of some ZA modes in the Γ-M branch (at about one-fourth of the branch) oscillates strongly with the number of neighbors included, and can even become imaginary when less than 13 are used, resulting in an instability of the crystal. Also, the K_{TO} mode keeps decreasing in going from 20 to 30 neighbors, though the effect remains small (8–9 cm^{-1}). This drift signals the presence of a Kohn anomaly,[63] at the K point of the Brillouin zone the electronic band gap vanishes and a singularity arises in the highest optical phonon mode. A detailed discussion is offered in Ref. 29.

IV. THERMODYNAMIC PROPERTIES

We present in this final section our results on the thermodynamic properties of diamond, graphite and graphene using the quasiharmonic approximation and phonon dispersions at the GGA level. As outlined in Sec. II B we first perform a direct minimization over the lattice parameter(s) $\{a_i\}$ of the vibrational free energy $F(\{a_i\}, T)$ [Eq. (8)]. This gives us, at any temperature T, the equilibrium structure, shown in Figs. 11, 12, and 13. For diamond and graphene, we use in Eq. (8) the equations of state obtained from the ground state calculations presented in Sec. III A. For graphite this choice would not be useful or accurate, since the theoretical c/a is much larger than the experimental one. So we force the equation of state to be a minimum for $c/a = 2.725$ and $a = 4.65$ a.u. (fixing only c/a and relaxing a would give $a = 4.66$ a.u., with negligible effects on the thermal expansion). In particular, our "corrected" equation of state is obtained by fitting with a fourth order polynomial the true equation of state around the experimental a and c/a, and then dropping from this polynomial the linear order terms. Since the second derivatives of the polynomial remain unchanged, we keep the elastic constants unchanged, and the only input from experiments remains the c/a ratio. We have also checked the
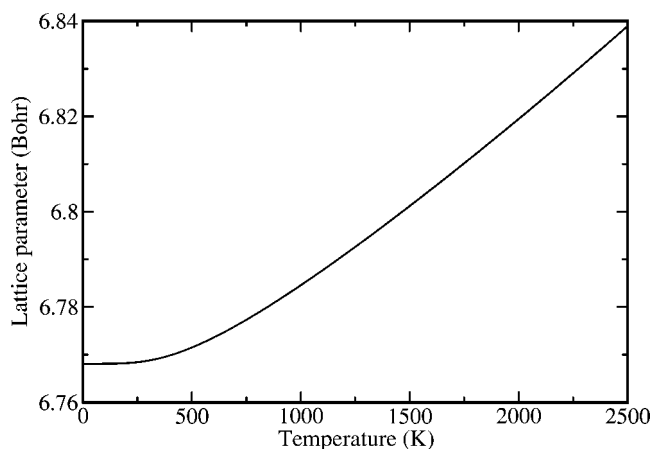
FIG. 11. Lattice parameter of diamond as a function of temperature.

effects of imposing to C_{13} its experimental value (C_{13} is the elastic constant that is predicted least accurately), but the changes were small.

The dependence of the phonon frequencies on the lattice parameters is determined by calculating the whole phonon dispersions at several values and interpolating these in between. For diamond and graphene we use four different values of a (from 6.76 to 6.85 a.u. for diamond, and from 4.654 to 4.668 a.u. for graphene) and interpolate them with a cubic polynomial. For graphite, where two independent structural parameters are needed, we restrict ourselves to linear interpolations and calculate the phonon dispersions for the three combinations $(a, c/a) = (4.659, 2.725)$, $(4.659, 2.9)$, and $(4.667, 2.725)$.

Before focusing on the thermal expansion, we examine the zero-point motion. Indeed, the effects of temperature up to about 1000 K remains small or comparable to the zero-point expansion of the lattice parameters. In diamond, once the zero-point motion is added the equilibrium lattice parameter a expands from 6.743 a.u. to 6.768 a.u., a difference of 0.4%. For graphene, a changes from 4.654 a.u. to 4.668 a.u. with zero-point motion corrections ($+0.3\%$); for graphite a increases from 4.65 to 4.664 a.u. ($+0.3\%$) and c from 12.671 to 12.711 ($+0.3\%$). The increase is similar in each
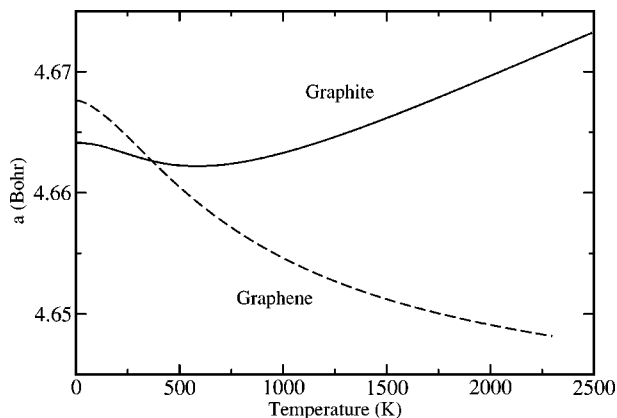
FIG. 12. In-plane lattice parameter of graphite (solid line) and graphene (dashed line) as a function of temperature.
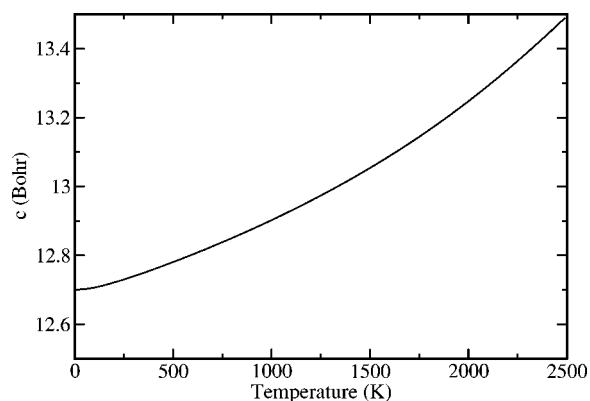

FIG. 13. Out-of-plane lattice parameter of graphite as a function of temperature.

case, and even comparable to the discrepancy between experiments and GGA or LDA ground states.

The coefficients of linear thermal expansion at any temperature are obtained by direct numerical differentiation of the previous data. Results are shown in Figs. 14, 15, and 16. For the case of diamond, we also plot the linear thermal expansion coefficient calculated using the Grüneisen formalism [Eq. (12)] instead of directly minimizing the free energy. While at low temperature the two curves agree, a discrepancy becomes notable above 1000 K, and direct minimization should be performed. This difference between the Grüneisen approach and a direct minimization seems to explain much of the discrepancy between the calculations of Ref. 11 and our results. Finally a Monte Carlo path integral study by Herrero and Ramírez,[64] which does not use the QHA, gives very similar results.

For graphite, the in-plane coefficient of linear thermal expansion slightly overestimates the experimental values, but overall the agreement remains excellent, even at high temperatures. Out-of-plane, the agreement holds well up to
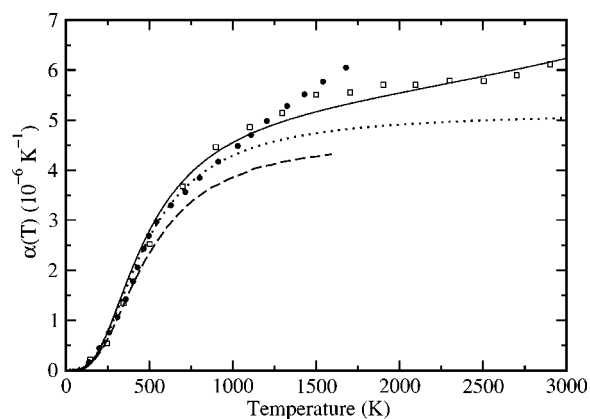

FIG. 14. Coefficient of linear thermal expansion for diamond as a function of temperature. We compare our QHA-GGA *ab initio* calculations (solid line) to experiments (Ref. 10, filled circles), a path integral Monte Carlo study using a Tersoff empirical potential (Ref. 64, open squares) and the QHA-LDA study by Pavone *et al.* (Ref. 11) (dashed line). The QHA-GGA thermal expansion calculated using the Grüneisen equation [Eq. (12)] is also shown (dotted line).
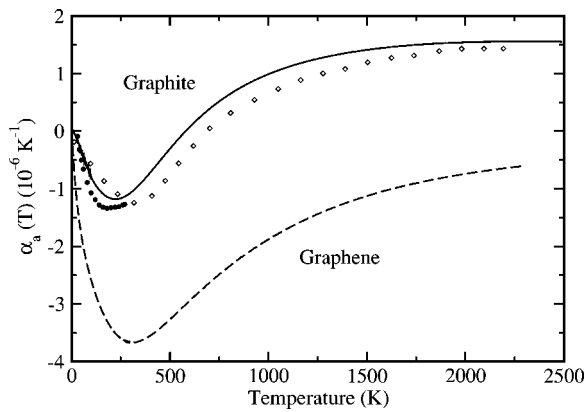
FIG. 15. In-plane coefficient of linear thermal expansion as a function of temperature for graphite (solid line) and graphene (dashed line) from our QHA-GGA *ab initio* study. The experimental results for graphite are from Ref. 14 (filled circles) and Ref. 7 (open diamonds).

150 K, after which the coefficient of linear thermal expansion is underestimated by about 30% at 1000 K.

In-plane, the coefficient of linear thermal expansion is confirmed to be negative from 0 to about 600 K. This feature, absent in diamond, is much more apparent in graphene, where the coefficient of linear thermal expansion keeps being negative up to 2300 K. This thermal contraction will likely appear also in single-walled nanotubes (one graphene sheet rolled on itself).[65] Some molecular dynamics calculations[41,66] have already pointed out this characteristic of SWNTs.

To further analyze thermal contraction, we show in Figs. 17 and 18 the in-plane mode Grüneisen parameters of graphene and graphite (see Sec. II B). These are obtained from an interpolation of the phonon frequencies with a quadratic (or linear, for graphite) polynomial in the lattice constant(s), and computed at the ground state geometry. Whereas in diamond the Grüneisen parameters (calculated in Refs. 11 and 20) were shown to be all positive, in graphite and graphene some bands display large and negative Grüneisen parameters (we have used the definition $\gamma_j(\mathbf{q})$
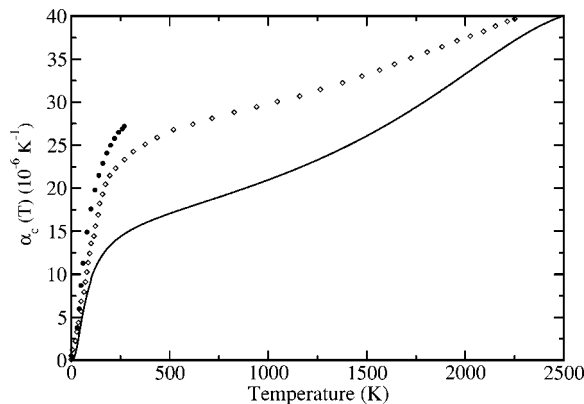

FIG. 16. Out-of-plane coefficient of linear thermal expansion as a function of temperature for graphite from our QHA-GGA *ab initio* study (solid line). The experimental results are from Ref. 14 (filled circles) and Ref. 7 (open diamonds).
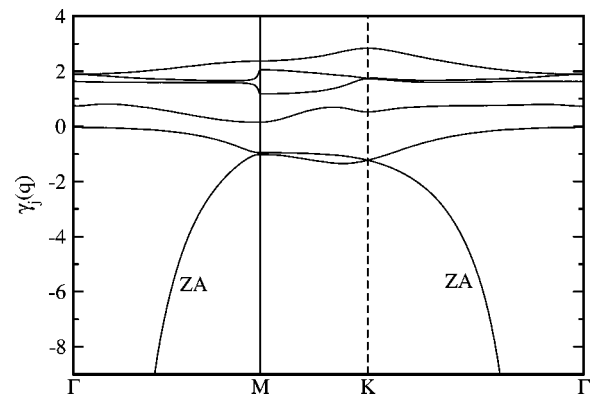

FIG. 17. *Ab initio* mode Grüneisen parameters for graphene.

$=-[a/2\omega_j(\mathbf{q})][d\omega_j(\mathbf{q})/da])$. While not visible in the figure, the Grüneisen parameters for the lowest acoustic branch of graphite become as low as -40, and as low as -80 in graphene. Therefore, at low temperatures (where most optical modes with positive Grüneisen parameters are still not excited) the contribution from the negative Grüneisen parameters will be dominant and thermal expansion [from Eq. (12)] negative.

The negative Grüneisen parameters correspond to the lowest transversal acoustic (ZA) modes, and in the case of graphite to the (ZO′) modes as well, which can be described as "acoustic" inside the layer and optical out-of-plane (see Sec. III B). Indeed, the phonon frequencies for such modes increase when the in-plane lattice parameter is increased, contrary to the usual behavior, since upon stretching atoms in the layer will be less free to move in the z direction (just like a string that is stretched will have vibrations of smaller amplitude and higher frequency). The eigenvector corresponding to the ZA mode at $\mathbf{q}=2\pi/a(0,0.1,0)$ is represented in Fig. 19. In graphite the Grüneisen parameters of these modes are less negative as a consequence of stacking that directly affects the out-of-plane vibrations. The thermal contraction is found to be greatly reduced with respect to graphene.

This phenomenon, named "membrane effect," was predicted by Lifshitz[61] in 1952, when he pointed out the role of the ZA modes (also called bending modes) in membranes and layered materials. In particular, several recent studies
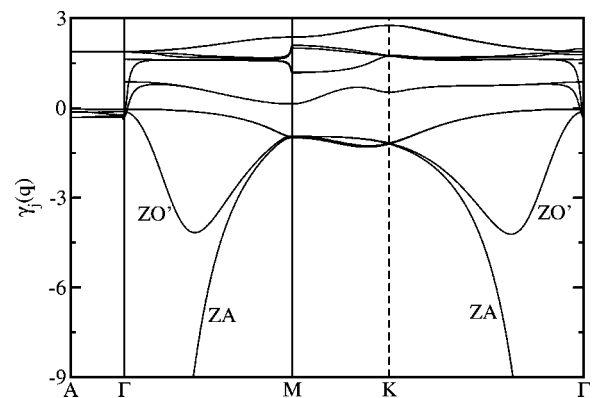

FIG. 18. *Ab initio* in-plane mode Grüneisen parameters for graphite.
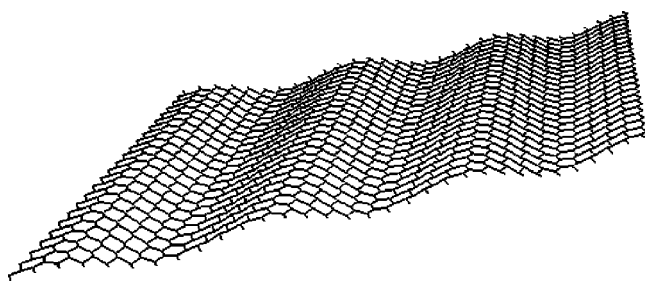
FIG. 19. ZA bending mode of a graphene sheet.

have highlighted the relevance of these modes to the thermal properties of layered crystals such as graphite, boron nitride, and gallium sulfide.[67–69]

Other relevant thermodynamic quantities can also be calculated from the vibrational free energy. For example, the dependence of elastic constants on temperature can be derived from the second derivatives of the free energy [Eq. (8)] taken at the respective minimum for any given T. Our results are shown in Figs. 20 and 21 (diamond and graphite, respectively). Again, the zero-point motion has a significant effect on the elastic constants; the agreement with experimental data for the temperature dependence of the bulk modulus of diamond is excellent (upper panel of Fig. 20). We note that the temperature dependence of the bulk modulus of diamond has already been obtained by Karch *et al.*[70] using LDA calculations.

Finally, in Figs. 22–24 we present results on the heat capacities for all the systems considered, both at constant volume (C_v) and constant pressure (C_p). C_v is computed using Eq. (14), in which we use at each temperature T the interpolated phonon frequencies calculated at the lattice constant(s) that minimize the respective free energy. To obtain C_p, we add to C_v the additional term $C_p - C_v = TV_0 B_0 \alpha_V^2$ where V_0 is the unit cell volume, α_V the volumetric thermal expansion and B_0 the bulk modulus. All these quantities are taken from

FIG. 21. Elastic constants of graphite ($C_{11}+C_{12}, C_{13}, C_{33}$) and bulk modulus ($B_0$) as a function of temperature. The filled circles (at 0 K) indicate their ground state values (as in Table II) before accounting for zero-point motion.

our *ab initio* results and evaluated at each of the temperatures considered. The difference between C_p and C_v is small, at most about 2% of the value of C_v for graphite and 5% for diamond. Note that C_p and C_v shown on the figures are normalized by dividing by the unit cell mass.

The heat capacity of diamond, graphite, and graphene are almost identical except at very low temperatures, in a manifestation of the law of corresponding states for different materials with essentially very similar Debye temperature. Agreement with experimental data of diamond and graphite is very good.

V. CONCLUSIONS

We have presented a full first-principles study of the structural, vibrational, and thermodynamic properties of diamond, graphite, and graphene at the GGA-PBE level and using the quasiharmonic approximation to derive the finite-temperature behavior of several thermodynamic quantities. All our results are in very good agreement with experimental data, the phonon dispersions are well reproduced, as well as
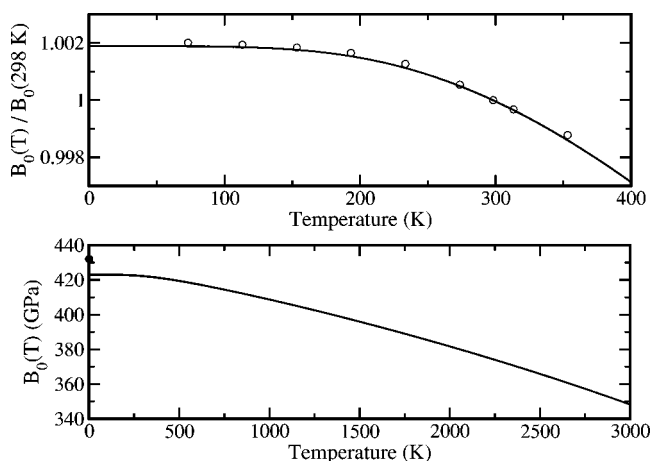

FIG. 20. Lower panel, bulk modulus $B_0(T)$ of diamond as a function of temperature. The filled circle indicates the value of the bulk modulus (as in Table I) before accounting for zero-point motion. Upper panel, theoretical (solid line) and experimental values (Ref. 71, open circles) for the ratio between $B_0(T)$ and $B_0(298 \text{ K})$ in the low-temperature region.
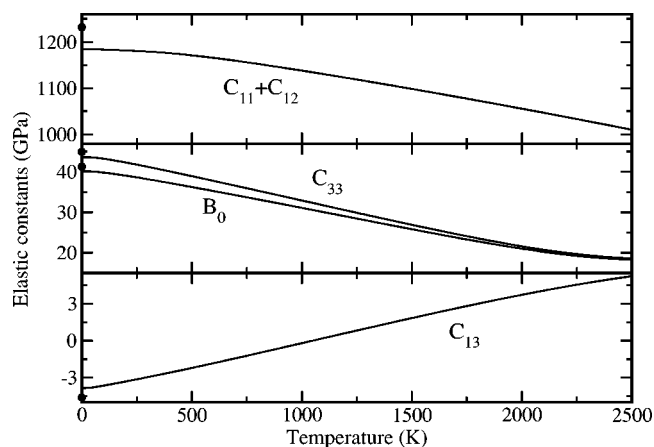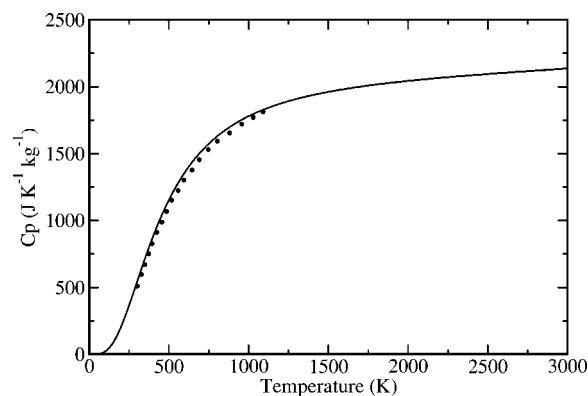

FIG. 22. Constant pressure heat capacity for diamond (solid line). Experimental results are from Refs. 49 and 72 (circles), as reported by Ref. 64.
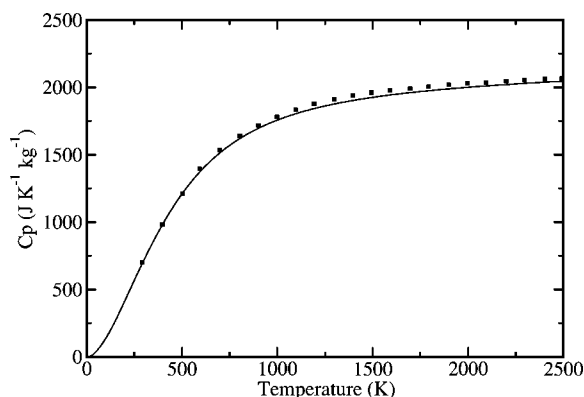
FIG. 23. Constant pressure heat capacity for graphite (solid line). Experimental results are from Ref. 73 (squares), as reported by Ref. 74.
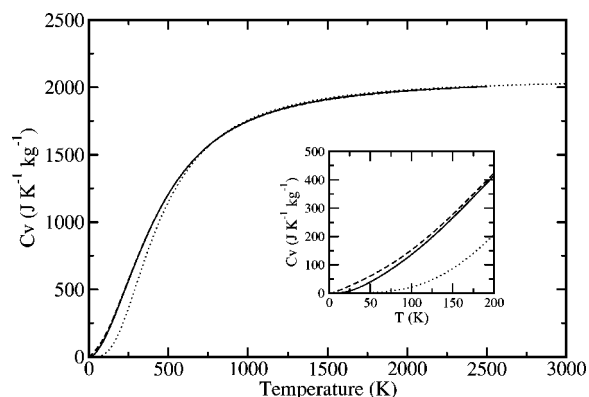

FIG. 24. Constant volume heat capacity for graphite (solid line), graphene (dashed line), and diamond (dotted line). The inset shows an enlargement of the low-temperature region.

most of the elastic constants. In graphite, the C_{33} elastic constant and the Γ to A phonon dispersions are found to be in good agreement with experimental results provided the calculations are performed at the experimental c/a. Only the C_{13} constant remains in poor agreement with experimental data.

The decay of the long-ranged interatomic force constants has been analyzed in detail. It has been shown that interactions in the (110) direction in diamond are longer-ranged than those in other directions, as is characteristic of the zinc-blende and diamond structures. For graphene and graphite, in-plane interactions are even longer ranged and the phonon frequencies sensitive to the truncation of the interatomic force constants.

Thermodynamic properties such as the thermal expansion, temperature dependence of elastic moduli, and specific heat have been calculated in the quasiharmonic approximation. These quantities are all found to be in close agreement with experiments, except for the out-of-plane thermal expansion of graphite at temperatures higher than 150 K. Graphite shows a distinctive in-plane negative thermal-expansion coefficient that reaches the minimum around room temperature, again in very good agreement with experiments. This effect is found to be three times as large in graphene. In both cases, the mode Grüneisen parameters show that the ZA bending acoustic modes are responsible for the contraction, in a direct manifestation of the membrane effect predicted by Lifshitz[61] in 1952. These distinctive features will likely affect the thermodynamic properties of single-walled and multiwalled carbon nanotubes.[41,65,66]

ACKNOWLEDGMENTS

---

*Electronic address: nicolas.mounet@polytechnique.org

†URL: http://nnn.mit.edu/

[1] K. S. Novoselov, A. K. Geim, S. V. Morozov, D. Jiang, Y. Zhang, S. V. Dubonos, I. V. Grigorieva, and A. A. Firsov, Science **306**, 666 (2004).

[2] R. J. Chen, S. Bangsaruntip, K. A. Drouvalakis, N. W. S. Kam, M. Shim, Y. Li, W. Kim, P. J. Utz, and H. Dai, Proc. Natl. Acad. Sci. U.S.A. **100**, 4984 (2003).

[3] G. Galli, R. M. Martin, R. Car, and M. Parrinello, Phys. Rev. Lett. **63**, 988 (1989).

[4] G. Galli, R. M. Martin, R. Car, and M. Parrinello, Phys. Rev. Lett. **62**, 555 (1989).

[5] A. De Vita, G. Galli, A. Canning, and R. Car, Nature (London) **379**, 523 (1996).

[6] *Graphite and Precursors*, edited by P. Delhaes (Gordon and Breach, Australia, 2001), Chap. 6.

[7] H. O. Pierson, *Handbook of Carbon, Graphite, Diamond, and Fullerenes: Properties, Processing, and Applications* (Noyes Publications, Park Ridge, NJ, 1993), pp. 59–60.

[8] R. Saito, G. Dresselhaus, and M. S. Dresselhaus, *Physical Properties of Carbon Nanotubes* (Imperial College Press, London, 1998).

[9] J. L. Warren, J. L. Yarnell, G. Dolling, and R. A. Cowley, Phys. Rev. **158**, 805 (1967).

[10] G. A. Slack and S. F. Bartram, J. Appl. Phys. **46**, 89 (1975).

[11] P. Pavone, K. Karch, O. Schütt, W. Windl, D. Strauch, P. Giannozzi, and S. Baroni, Phys. Rev. B **48**, 3156 (1993).

[12] J. Maultzsch, S. Reich, C. Thomsen, H. Requardt, and P. Ordejón, Phys. Rev. Lett. **92**, 075501 (2004).

[13] L. Wirtz and A. Rubio, Solid State Commun. **131**, 141 (2004).

[14] A. C. Bailey and B. Yates, J. Appl. Phys. **41**, 5088 (1970).

[15] J. B. Nelson and D. P. Riley, Proc. Phys. Soc. London **57**, 477 (1945).

[16] S. Baroni, S. de Gironcoli, A. Dal Corso, and P. Giannozzi, Rev.

Mod. Phys. **73**, 515 (2001).

[17] P. Giannozzi, S. de Gironcoli, P. Pavone, and S. Baroni, Phys. Rev. B **43**, 7231 (1991).

[18] D. Vanderbilt, Phys. Rev. B **41**, R7892 (1990).

[19] J. P. Perdew, K. Burke, and M. Ernzerhof, Phys. Rev. Lett. **77**, 3865 (1996).

[20] J. Xie, S. P. Chen, J. S. Tse, S. de Gironcoli, and S. Baroni, Phys. Rev. B **60**, 9444 (1999).

[21] F. Favot and A. Dal Corso, Phys. Rev. B **60**, 11 427 (1999).

[22] J. C. Boettger, Phys. Rev. B **55**, 11 202 (1997).

[23] M. C. Schabel and J. L. Martins, Phys. Rev. B **46**, 7185 (1992).

[24] O. Dubay and G. Kresse, Phys. Rev. B **67**, 035401 (2003).

[25] P. Pavone, R. Bauer, K. Karch, O. Schutt, S. Vent, W. Windl, D. Strauch, S. Baroni, and S. de Gironcoli, Physica B **219/220**, 439 (1996).

[26] L. H. Ye, B. G. Liu, D. S. Wang, and R. Han, Phys. Rev. B **69**, 235409 (2004).

[27] I. H. Lee and R. M. Martin, Phys. Rev. B **56**, 7197 (1997).

[28] K. R. Kganyago and P. E. Ngoepe, Mol. Simul. **22**, 39 (1999).

[29] S. Piscanec, M. Lazzeri, F. Mauri, A. C. Ferrari, and J. Robertson, Phys. Rev. Lett. **93**, 185503 (2004).

[30] P. Pavone, Ph.D. thesis, SISSA, Trieste, Italy, 1991.

[31] H. Rydberg, M. Dion, N. Jacobson, E. Schroder, P. Hyldgaard, S. I. Simak, D. C. Langreth, and B. I. Lundqvist, Phys. Rev. Lett. **91**, 126402 (2003).

[32] W. Kohn, Y. Meir, and D. E. Makarov, Phys. Rev. Lett. **80**, 4153 (1998).

[33] W. Kohn and L. J. Sham, Phys. Rev. **140**, A1133 (1965).

[34] P. Hohenberg and W. Kohn, Phys. Rev. **136**, B864 (1964).

[35] S. Baroni, P. Giannozzi, and A. Testa, Phys. Rev. Lett. **58**, 1861 (1987).

[36] S. de Gironcoli, Phys. Rev. B **51**, 6773 (1995).

[37] A. A. Maradudin, E. W. Montroll, and G. H. Weiss, *Theory of Lattice Dynamics in the Harmonic Approximation* (Academic, New York, 1963), Vol. 3 of Solid-state physics, pp. 45–46.

[38] A. A. Quong and A. Y. Liu, Phys. Rev. B **56**, 7767 (1997).

[39] S. Narasimhan and S. de Gironcoli, Phys. Rev. B **65**, 064302 (2002).

[40] T. H. K. Barron, J. G. Collins, and G. K. White, Adv. Phys. **29**, 609 (1980).

[41] P. K. Schelling and P. Keblinski, Phys. Rev. B **68**, 035425 (2003).

[42] S. Baroni *et al.*, http://www.pwscf.org

[43] http://www.gnu.org/copyleft/gpl.html

[44] A. Dal Corso, *C.pbe-rrkjus.upf*, http://www.pwscf.org/pseudo/1.3/UPF/C.pbe-rrkjus.UPF

[45] A. M. Rappe, K. M. Rabe, E. Kaxiras, and J. D. Joannopoulos, Phys. Rev. B **41**, R1227 (1990).

[46] J. P. Perdew and A. Zunger, Phys. Rev. B **23**, 5048 (1981).

[47] N. Marzari, D. Vanderbilt, A. De Vita, and M. C. Payne, Phys. Rev. Lett. **82**, 3296 (1999).

[48] E. Ziambaras and E. Schröder, Phys. Rev. B **68**, 064112 (2003).

[49] *Physics of Group IV and III-V Compounds*, edited by O. Madelung (Springer-Verlag, Berlin, 1982), Vol. 17a of Landolt-Börnstein, New Series, Group III, p. 107.

[50] M. H. Grimsditch and A. K. Ramdas, Phys. Rev. B **11**, 3139 (1975).

[51] Y. X. Zhao and I. L. Spain, Phys. Rev. B **40**, 993 (1989).

[52] M. Hanfland, H. Beister, and K. Syassen, Phys. Rev. B **39**, 12 598 (1989).

[53] J. Donohue, *The Structures of the Elements* (Kreiger, Malabar, 1982), p. 256.

[54] O. L. Blakslee, D. G. Proctor, E. J. Seldin, G. B. Spence, and T. Weng, J. Appl. Phys. **41**, 3373 (1970).

[55] C. Oshima, T. Aizawa, R. Souda, Y. Ishizawa, and Y. Sumiyoshi, Solid State Commun. **65**, 1601 (1988).

[56] S. Siebentritt, R. Pues, K.-H. Rieder, and A. M. Shikin, Phys. Rev. B **55**, 7927 (1997).

[57] H. Yanagisawa, T. Tanaka, Y. Ishida, M. Matsue, E. Rokuta, S. Otani, and C. Oshima, Surf. Interface Anal. **37**, 133 (2005).

[58] R. Nicklow, N. Wakabayashi, and H. G. Smith, Phys. Rev. B **5**, 4951 (1972).

[59] F. Tuinstra and J. L. Koenig, J. Chem. Phys. **53**, 1126 (1970).

[60] H. Zabel, J. Phys.: Condens. Matter **13**, 7679 (2001).

[61] I. M. Lifshitz, Zh. Eksp. Teor. Fiz. **22**, 475 (1952).

[62] C. Kittel, *Introduction to Solid State Physics* (Wiley, New York, 1976), Chap. 3, 5th ed.

[63] W. Kohn, Phys. Rev. Lett. **2**, 393 (1959).

[64] C. P. Herrero and R. Ramírez, Phys. Rev. B **63**, 024103 (2000).

[65] N. Mounet and N. Marzari (unpublished).

[66] Y. K. Kwon, S. Berber, and D. Tománek, Phys. Rev. Lett. **92**, 015901 (2004).

[67] G. L. Belenkii, R. A. Suleimanov, N. A. Abdullaev, and V. Y. Stenshraiber, Sov. Phys. Solid State **26**, 2142 (1984).

[68] N. A. Abdullaev, Phys. Solid State **43**, 727 (2001).

[69] N. A. Abdullaev, R. A. Suleimanov, M. A. Aldzhanov, and L. N. Alieva, Phys. Solid State **44**, 1859 (2002).

[70] K. Karch, T. Dietrich, W. Windl, P. Pavone, A. P. Mayer, and D. Strauch, Phys. Rev. B **53**, 7259 (1996).

[71] H. J. McSkimin and P. Andreatch, J. Appl. Phys. **43**, 2944 (1972).

[72] A. C. Victor, J. Chem. Phys. **36**, 1903 (1962).

[73] R. R. Hultgren, *Selected Values of the Thermodynamic Properties of the Elements* (American Society for Metals, Metals Park, OH, 1973).

[74] L. E. Fried and W. M. Howard, Phys. Rev. B **61**, 8734 (2000).